HHS Public Access

Author manuscript

Curr Biol. Author manuscript; available in PMC 2023 May 09.

Published in final edited form as:

Curr Biol. 2022 May 09; 32(9): 2084–2092.e4. doi:10.1016/j.cub.2022.03.007.

Cullin-5 mutants reveal collective sensing of the nucleocytoplasmic ratio in *Drosophila* embryogenesis

Luke Hayden[1], **Anna Chao**[1], **Victoria E. Deneke**[1,^], **Massimo Vergassola**[2,3], **Alberto Puliafito**[4,5], **Stefano Di Talia**[1,6,*]

[1]Department of Cell Biology, Duke University School of Medicine, Durham, NC 27710, USA

[2]Laboratoire de physique de l'École Normale Supérieure, CNRS, PSL Research University, Sorbonne Université, Paris, France

[3]Department of Physics, University of California, San Diego, La Jolla, CA, USA

[4]Candiolo Cancer Institute, FPO-IRCCS, Laboratory of Cell Migration, Candiolo, 10060, Italy

[5]Department of Oncology, Università di Torino, Candiolo, 10060, Italy

[6]Lead contact

Summary

In most metazoans, early embryonic development is characterized by rapid division cycles which pause before gastrulation at the mid-blastula transition (MBT).[1] These cleavage divisions are accompanied by cytoskeletal rearrangements which ensure proper nuclear positioning. Yet, the molecular mechanisms controlling nuclear positioning are not fully elucidated. In *Drosophila*, early embryogenesis unfolds in a multinucleated syncytium. Nuclei rapidly move across the anterior-posterior (AP) axis at cell cycles 4–6 in a process driven by actomyosin contractility and cytoplasmic flows.[2,3] In *shackleton* (*shkl*) mutants, this axial spreading is impaired.[4] Here, we show that *shkl* mutants carry mutations in the *cullin-5* (*cul-5*) gene. Live imaging experiments show that Cul-5 is downstream of the cell cycle but required for cortical actomyosin contractility. The nuclear spreading phenotype of *cul-5* mutants can be rescued by reducing Src activity, suggesting that a major target of Cul-5 is Src kinase. *cul-5* mutants display gradients of nuclear

*Correspondence: stefano.ditalia@duke.edu.

^Present address: Research Institute of Molecular Pathology (IMP), Vienna BioCenter (VBC), Campus-Vienna-Biocenter 1, 1030 Vienna, Austria

Author contributions

Conceptualization, L.H., A.C., V.E.D., M.V., and S.D.; Methodology, L.H., A.C., V.E.D., M.V., A.P., and S.D.; Software, L.H., A.P., and S.D.; Investigation, L.H., A.C., V.E.D., A.P., and S.D.; Writing – Original Draft, L.H. and S.D.; Supervision, A.C and S.D. Funding Acquisition, S.D.

Inclusion and Diversity

One or more of the authors of this paper self-identifies as an underrepresented ethnic minority in science. One or more of the authors of this paper received support from a program designed to increase minority representation in science. While citing references scientifically relevant for this work, we also actively worked to promote gender balance in our reference list.

Declaration of interests

The authors declare no competing interests.

density across the AP axis which we exploit to study cell cycle control as a function of the N/C ratio. We found that the N/C ratio is sensed collectively in neighborhoods of about 100μm and such collective sensing is required for a precise MBT in which all the nuclei in the embryo pause their division cycle. Moreover, we found that the response to the N/C ratio is slightly graded along the AP axis. These two features can be linked to Cdk1 dynamics. Collectively, we reveal a new pathway controlling nuclear positioning and provide a dissection of how nuclear cycles respond to the N/C ratio.

eTOC Blurb

Hayden et al show that the ubiquitin ligase Cullin-5 is important for cortical actomyosin contractility and nuclear positioning in *Drosophila* embryos. Moreover, the authors reveal that the decision of nuclei to lengthen the cell cycle at the mid-blastula transition is made in large collectives and mediated by Cdk1 reaction-diffusion dynamics.

Keywords

Nuclear positioning; actomyosin contractility; Mid-blastula transition; nuclear-to-cytoplasmic ratio; Cullin-5; Src

Results

shkl encodes the ubiquitin ligase *cullin-5*

shkl mutants are among the few available genetic perturbations which directly impinge on the spreading of nuclei in early *Drosophila* embryogenesis.[4,5] Moreover, *shkl* embryos display gradients in nuclear density, which have been linked to a significant decrease in the synchrony of the last cell cycle preceding the MBT.[3] To elucidate how *shkl* regulates nuclear positioning and how such regulation impacts cell cycle lengthening at the MBT, we first obtained two *shkl* alleles identified in the original mutagenesis screen (*shkl*^{GM130} and *shkl*^{GM163}) and imaged embryos laid by transheterozygous mothers (hereinafter *shkl* embryos). We confirmed that in *shkl* embryos the nuclear cloud failed to reach the posterior pole of the embryo at the correct time and nuclei were not positioned uniformly, as seen previously (Figure 1A–B).[4] Moreover, we found that the lower density of nuclei in the posterior of the embryo was frequently accompanied by an extra round of nuclear divisions (Video S1). Thus, failures in nuclear positioning can have significant impact on the decision of nuclei to lengthen the cell cycle at the MBT.

To identify the *shkl* gene, we used a DNA sequencing approach, centered on the fact that the original screen was performed in a strain carrying an isogenic third chromosome and that two alleles of the *shkl* gene were available.[4] We reasoned that the third chromosomes of these two alleles had little time (~20 years) to accumulate mutations with respect to each other. Thus, we predicted that genomic sequencing of *shkl* flies (*shkl*^{GM130}/*shkl*^{GM163}) would show a much lower number of heterozygous single nucleotide polymorphisms (SNPs) than homozygous ones relative to the reference genome on the third chromosome, a prediction which we readily confirmed (Figure 1C). Taking advantage of the low number of heterozygous SNPs and the previous mapping[4] of *shkl* between two markers (*ebony*

and *claret*) on the right arm of chromosome 3, we looked for genes that carried two heterozygous missense SNPs with the idea that this would narrow our search to only a handful of genes (Figure 1D). Bioinformatics analysis confirmed the validity of this argument, and we identified *cullin-5* (Cul-5) as the best candidate as allele *shkl*^{GM163} carried a premature stop codon at amino acid 51 and *shkl*^{GM130}, a missense mutation (E to K) in the very conserved neddylation domain, a domain required for ubiquitin ligase activity and which is well-conserved across evolution (Figure 1E).[6] To perform complementation and rescue experiments, we fixed and stained embryos with DAPI to estimate the extent of nuclear spreading by measuring the shape of the nuclear cloud in cell cycle (cc) 6. We found that *shkl* alleles failed to complement an available *cullin-5* mutant (Figure 1F). In addition, maternal expression of *cullin-5* from the *twine* promoter (which drives expression specifically in the germline[7]) was able to significantly rescue the nuclear spreading defects (Figure 1F). Collectively, these results identify *shkl* mutants as alleles of the *cullin-5* genes and demonstrate that maternal expression of *cullin-5* is important for nuclear positioning in *Drosophila* embryos.

shkl is downstream of the cell cycle and regulates cortical contractility

In our previous work, we showed that nuclear spreading is driven by cytoplasmic flows generated by cortical actomyosin contractility, which is in turn controlled spatiotemporally by the cell cycle oscillator (Figure 2A).[3] To quantify the degree to which cytoplasmic flows are disrupted in *shkl* embryos, we used yolk autofluorescence images to perform particle image velocimetry (PIV) in live embryos also expressing PCNA-TagRFP (which allows visualization of nuclei deep in the embryo) and measured the velocity of the cytosol and nuclei during the early cell cycles when axial expansion occurs. As previously shown, the wildtype embryos showed strong cytoplasmic flows coupled with nuclear movement which spread the nuclei across the anterior-posterior (AP) axis by the end of cc 6 (Figure 2B, D, S1).[3] In contrast, cytoplasmic flows and nuclear movement in *shkl* embryos were sharply reduced (Figure 2C, E, S1). Since cytoplasmic flows are generated by recruitment of active Myosin II to the cortex by active Rho,[3,8] we sought to determine if the activities of these regulators are perturbed in *shkl* embryos. To that end, we measured the dynamics of a Rho biosensor[9] and myosin II recruitment to the embryo cortex. Both Rho activity (Figure 2F, S1) and myosin II recruitment (Figure 2G) were reduced in *shkl* embryos as compared to wildtype. Next, we analyzed whether Cul-5 might impact actomyosin contractility by regulating the cell cycle. To this end, we measured the Cdk1-to-PP1 activity ratio using a FRET-based biosensor in both wildtype and *shkl* embryos.[10,11] The oscillations in the activity ratio were similar in wildtype and *shkl* embryos. Moreover, the duration of the cell cycle near the middle of the embryo was also essentially unaltered (Figure 2H, S2). Therefore, we argue that Cul-5 does not regulate the cell cycle oscillator. Taken together, our results indicate that Cul-5 is necessary for the proper activity of Rho and recruitment of myosin II which in turn regulate cortical contractility and nuclear positioning.

Cul-5 regulates cortical contractility through restricting the activity of Src.

Cul-5 is a ubiquitin ligase which works in conjunction with other factors to regulate protein stability.[12] A major target of Cul-5 is Src kinase[13–15], whose activity is restricted by several ubiquitin ligases.[16–18] Src is known to regulate the cytoskeleton[19,20], including actomyosin

contractility.[21] These observations suggest that Cul-5 could (at least partly) regulate the axial expansion process by restricting Src activity. To test this hypothesis, we performed experiments using the Gal4/UAS system to overexpress constitutively active forms of the two Src homologs in *Drosophila*, Src42A or Src64B.[22] We saw that overexpression of either homolog is sufficient to recapitulate the *shkl* phenotype with sharply reduced cytoplasmic flows and nuclear spreading (Fig S1). Similarly, if *shkl* embryos have reduced cortical contractions due to excessive Src activity, then genetically decreasing Src activity should rescue the *shkl* phenotype. We examined *shkl* mutants also carrying only one functional copy of Src64B (heterozygous for $Src64B^{KO}$, described previously[20]) and quantified cytoplasmic flows and nuclear positioning. We saw that reducing Src activity in *shkl* embryos significantly reduced the defects in axial expansion (Figure 1F). Collectively, these results implicate the Cul-5/Src cascade in the regulation of nuclear positioning in *Drosophila* embryos.

Nuclei sense the local nuclear density in large groups to determine whether to divide

In wildtype embryos, the morphogenetic processes driving nuclear positioning ensure that nuclear density is rather uniform across the embryo.[3] Since nuclear divisions are synchronized within minutes[10,23] by Cdk1 waves,[10,24] nuclear density increases in 2-fold increments, which likely facilitates the consistent cell cycle lengthening observed in all nuclei at the MBT. To gain insights on how the embryo can achieve a robust response to changes in the N/C ratio, we observed that the nuclear spreading defects in *shkl* embryos cause a nuclear density gradient across the AP axis with lower density at the posterior (Figure 3A–B, Figure 4B). Therefore, we exploited this gradient to probe the response to gradual changes in nuclear density. We observed that the lower density of nuclei in the posterior of the embryo is frequently accompanied by an extra round of nuclear division (Figure 3C). Interestingly, the size of the region which does an extra division varies across embryos and is frequently less than half the size of the embryo. Moreover, a salt-and-pepper phenotype with many regions of extra divisions next to regions of normal divisions is never observed.[25–27] These two observations suggest that the nuclei do not sense the N/C ratio globally or in an autonomous manner, but rather they do so in a collective manner over some distance, here called the community radius. To infer this radius, we divided embryos into grids, measured the nuclear density within circles of different radii, and scored whether each grid point was within a region of normal or extra division (Figure 3D). We then fit these curves to logistic equations and used the N/C ratio at which the curves crossed 50% probability as the best N/C ratio threshold predictor, above which we predict embryos do not divide (Figure 3E). As previously reported, these thresholds were around 70% of the wildtype cell cycle 14 nuclear densities.[25] This value is about half-way between the nuclear density at cell cycle 13 and 14, which likely contributes to the decision of all nuclei to divide rapidly at cell cycle 13 and lengthen their cycle 14. Next, we asked what is the fraction of nuclei that would fail to lengthen their cell cycle at the MBT as a function of the community radius. We found that to ensure that all nuclei (>99%) undergo a collective pause at the MBT, the response to the N/C ratio must be averaged over a community radius of at least 35μm (Figure 3F). Such a community would contain about one hundred nuclei, thus implying that a robust cell cycle decision at the MBT requires a collective nuclear response.

Next, we tried to infer the optimal radius and a possible molecular mechanism for the collective nature of the cell cycle decision. Using the estimated thresholds, we measured the proportion of correct predictions made in a test data set of *shkI* embryos with regions of extra division and saw a peak in the fraction of correct predictions at a community radius of about 70μm (Figure 3F). We used the Cdk1/PP1 FRET biosensor to measure the correlation length of the Cdk1/PP1 activity field. The correlation length can be estimated from the two-point correlation function, which measures how variables at different positions co-vary with one another. Specifically, we measure how Cdk1/PP1 activity at a position relates on average to Cdk1/PP1 activity at distance *x*. We found that the correlation length (about 100 μm) is similar to the optimal community radius, thus suggesting that the collective decision of nuclei to undergo an extra division or not might reflect the fact that Cdk1/PP1 activity in neighboring nuclei influences each other (Figure 3G). We have previously shown that spatial correlations in Cdk1/PP1 activity arise from the reaction-diffusion dynamics that drive the cell cycle during interphase.[24] To strengthen this argument, we performed numerical simulations of a mathematical model of Cdk1 activity[24] in the presence of spatially varying N/C ratios. Our model assumes that the N/C ratio locally sets different levels of activation of the DNA replication checkpoint, which feeds into Cdk1 activity via Chk1. The reaction-diffusion dynamics of Cdk1 activity then smoothen these inhomogeneities and result in nuclei collectively deciding whether to divide or not within regions of about 70 microns in radius (Figure 3H, S3). Thus, our model and experiments suggest a phenomenological mechanism for the N/C-based decision process that controls nuclear divisions. We conclude that the syncytial nature of the nuclear cycles coupled to the reaction-diffusion properties of the cell cycle oscillator ensure that nuclei act as large collectives and that such collectives increase the robustness of the MBT. Finally, we found that nuclear density can also predict the duration of cycle 13 in *shkI* embryos (Figure 3I and S3), in line with a model in which the N/C ratio sets the levels of Chk1 activation which, in turn, controls cell cycle duration.[10,28]

A gradient in sensing of the N/C ratio improves the ability to predict nuclear behaviors

While our previous results revealed the importance of collective N/C ratio sensing, we observed that the frequency of correct predictions from the model was limited to ~70% (Figure 3F), suggesting that we might be missing some additional regulation of the MBT or some additional aspects of the response to the N/C ratio. Thus, we sought to determine whether a more complex model, still centered on the N/C ratio, would account for the incorrect predictions (see Supplementary Figure 3). Notably, we found that the errors in prediction were distributed in a gradient across the AP axis (Figure 4A), suggesting that nuclei might sense the N/C ratio differently depending on their location. We therefore hypothesized that a slight gradient in the N/C ratio threshold (with some small variance between embryos) would be a better predictor (Figure 4B). With this model, we were able to correctly predict ~90% of nuclear divisions with the best community radius of ~100μm (Figure 4C). Moreover, most of the errors in this model accumulated very close to the border of the normal and extra division regions (Figure 4D), where we would expect that the ability of Cdk1 to propagate spatially might influence the decision.[10,24,29,30]

To further test the idea that the posterior of the embryo has a slightly higher N/C ratio threshold than the anterior, we compared the probability of nuclei dividing as a function of N/C ratio in the anterior and posterior. As predicted, the posterior third of the embryo showed a higher N/C ratio threshold than the anterior third (~8% higher, Figure 4E) which was independent of the community radius used (Figure 4F). To control that the apparent gradient in N/C ratio response is not due to cytoskeletal and/or other effects of reduced Cul-5 activity, we investigated the decision of nuclei to arrest at the MBT when the N/C ratio in embryos (with uniform nuclear positioning) is brought closer to the threshold by genetic manipulations. We reasoned that in these embryos the proximity of the nuclear density to the threshold will result in a significant fraction of embryos having an extra division. To this end, we imaged embryos generated by crossing wildtype females to males carrying compound chromosomes[25]. As a consequence, these embryos contained either one extra or one fewer copy of either chromosome 2 or 3. The embryos with one fewer copy of chromosome 2 or 3 have a DNA content (83% and 80% respectively) close to the 70% threshold seen in wildtype and also frequently had regions of an extra nuclear division.[25] As in *shkI* embryos, the posterior of the embryos featured a slightly higher threshold than the anterior (~2% increase for chromosome 2 and ~8% increase for chromosome 3; Figure 4G). In accordance, 100% (n=33) of extra divisions began in the posterior. The N/C ratio is an excellent predictor of the decision of nuclei to divide also in embryos with altered DNA content (Figure S4). However, the optimal threshold is shifted to higher values (~0.85, 11% higher than in wildtype; Figure 4G) which explains why a large number of extra divisions are observed in embryos with only one copy of chromosome 2 or 3. Since the community radius and the correlation length of the Cdk1/PP1 field are both ~100μm, we expect there to be a correlation between the Cdk1 activation rate measured during S phase (Figure 4H) and nuclear density in the compound chromosome embryos. Indeed, we saw there was a correlation between the two, and the regions of the embryo which underwent an extra division were clustered at a low DNA content and higher Cdk1 activation rate (Figure 4I).

To gain further insight on the slight gradient in the N/C ratio threshold across the AP axis, we divided wildtype embryos into grids and measured the Cdk1 activation rate in neighborhoods of each grid point at cc 13. We saw a slight but significant increase in the Cdk1 activation rate across the AP axis (Figure 4J) which was not due to differences in the N/C ratio (Figure S4). Since the increased duration of S phase at cc 13 is primarily due to the Cdk1 inhibition by Chk1[31–33], we measured the Cdk1 activation rate in *chk1 chk2* mutants and saw that the gradient across the AP axis was ablated (Figure 4K, S4). Thus, our results argue that the response of the cell cycle to nuclear density is not uniform across the embryo and that this difference might be dependent on the DNA replication checkpoint.

Discussion

The tight control of the cell cycle and nuclear (cell) positioning and number is a ubiquitous feature of metazoan development and is crucial to the proper development of early embryos. In this work we have taken advantage of *shkI* mutants which have defects in nuclear spreading to identify a novel pathway involved in the control of cortical contractility and gain insights into how nuclei respond to changes in the N/C ratio. Through DNA sequencing and complementation tests, we have identified *shkI* mutants as mutations of the ubiquitin

ligase Cul-5. In the early embryo, Cul-5 does not regulate the cell cycle oscillator but is required for Rho and myosin activity. Cul-5 restricts the levels of active Src kinase[13–15], which is a known regulator of the actomyosin cytoskeleton. Indeed, we found that the *cullin-5* phenotype could be largely rescued through a genetic reduction in Src activity and recapitulated through Src overexpression, indicating that a main function of Cul-5 is to downregulate Src activity. These results implicate the Cul-5/Src axis as a crucial pathway involved in the control of cortical contractility in early *Drosophila* embryos.

In the early embryo, nuclei regulate their own positioning through PP1 activity which spreads from the nuclei to the cortex.[3] This localized PP1 activity drives activation of Rho and Myosin II accumulation in turn.[3] Our results argue that Cul-5 and Src act in a pathway downstream or parallel to the cell cycle to regulate Rho activity. The molecular mechanisms by which Cul-5 and Src control Rho remain to be elucidated, as is the possible connection between the cell cycle oscillator and Cul-5/Src activities. Since Src has been shown to regulate Rho GTPases in several contexts,[34–36] these mechanisms are natural candidates for the regulation of cortical actomyosin regulation via the Cul-5/Src pathway.

Control of the MBT by the N/C ratio is important in several species, including *Drosophila* and *Xenopus*[25,26,37–40] but likely excluding zebrafish.[41–44] This density of DNA (as well as nuclear size[45,46]) can directly or indirectly impact multiple aspects of the MBT, namely zygotic gene expression[27,47–50] and cell cycle control.[26,28,37,51,52] Previous experiments with embryos irradiated to generate different nuclear densities across the AP axis argued that nuclear cycles and zygotic activation of a large set of genes respond to the local N/C ratio.[27] Here, we have exploited the changes in nuclear positioning in *shkI* embryos to generate a continuous range of nuclear densities. This property allowed us to gain insights into how the decision of nuclei to pause their cell cycles at the MBT is affected by the N/C ratio. We found that the threshold for nuclear division is about 70% of the density at nuclear cycle 14, which confirms previous results.[53] This value—about halfway between the density at cycle 13 and 14—likely contributes to the robustness of the MBT. However, it is not sufficient for the robustness of the MBT. To ensure reliable lengthening of cycle 14 in all nuclei, the sensing of the N/C ratio must be averaged over hundreds of nuclei. Consistently, our results suggest that nuclei sense the local N/C ratio in neighborhoods of ~100μm. This length essentially coincides with the correlation length of the Cdk1 activity field, which is established via reaction-diffusion mechanisms.[24] Additionally, we found that a model based on uniform sensing of the N/C ratio fails to predict the behavior of a large fraction of nuclei. However, a model assuming a slightly higher N/C ratio threshold in the posterior is highly predictable and mainly misses the behavior of nuclei at the interface between the region of extra division and that of normal division. Thus, we propose that the N/C ratio is the major regulator of the cell cycle at the MBT and that no mechanism other than a slight spatial modulation of the N/C threshold is needed to account for nuclear behaviors. This spatial modulation likely reflects the fact that the rate of Cdk1 activation is also slightly graded across the AP axis. The Cdk1 activation gradient is dependent on the DNA replication checkpoint, which argues that the gradient might be controlled by an asymmetric distribution of factors controlling DNA replication and/or Chk1 activity.[54–56] Alternatively, the DNA replication checkpoint and Cdk1 activity might be influenced by factors controlling AP patterning and expressed in gradients across the embryos.[57,58] In the future, it will

be interesting to understand the mechanisms and possible functional significance of this gradient.

The precise coordination of biochemical and mechanical signals is a ubiquitous feature of embryonic development. In early *Drosophila* embryogenesis, it is necessary for the uniform positioning of nuclei and timing of the MBT. Our work has identified a new pathway wherein Cul-5 regulates cortical contractility by restricting Src activity. Our results investigating embryos with patchy divisions indicate that nuclei sense the N/C ratio in neighborhoods of ~100μm and pause the cell cycle when the local density exceeds a threshold around 70% of the normal density at the MBT. Moreover, the threshold required to arrest the cell cycle is slightly graded across the AP axis and is coupled to the spatiotemporal dynamics of Cdk1. Quantitatively measuring biochemical and physical dynamics during specific morphogenic events will undoubtedly continue to reveal new insights into the mechanisms and regulations of these pathways.

STAR Methods

RESOURCE AVAILABILITY

Lead Contact—Further information and requests for resources and reagents should be directed to and will be fulfilled by the lead contact, Stefano Di Talia (stefano.ditalia@duke.edu).

Materials Availability—Newly generated fly lines in this study have not been deposited to a central repository but are available without restriction from the lead contact.

Data and Code Availability

- Genomic sequencing data have been deposited at NCBI Sequence Read Archive and are publicly available as of the date of publication. The accession number is listed in the key resources table. All other data reported in this paper will be shared by the lead contact upon request.
- All original code has been deposited at Github at the following link and is publicly available as of the date of publication: https://github.com/lhaydene26/Hayden_NCratio2022
- Any additional information required to reanalyze the data reported in this paper is available from the lead contact upon request.

EXPERIMENTAL MODEL AND SUBJECT DETAILS

Fly Lines and Husbandry—For all experiments, adult male and female flies of *Drosophila melanogaster* were raised at room temperature (~22°C) on standard molasses food without light/dark cycle. Prior to embryo collection, adult flies were moved to a 25°C incubator without light/dark cycle for a minimum of 2 days. Embryos were collected on apple juice agar plates with yeast paste from containers containing both male and female flies. Experiments in this study used embryos from ~cc 4 to cc 14/15 at the MBT at ~2h

of age, determined by examining nuclear numbers and movement. The fly lines used or generated in this study are described in the Key Resources Table.

METHOD DETAILS

Transgenic Line Construction—To construct the Cul-5 rescue line, cDNA for Cul-5 (FI20194) was obtained from the *Drosophila* Genomics Resource Center and cloned in plasmid pBabr containing the *twe* promotor and 3'UTR.[7] Transgenic flies were generated by phiC31 integrase-mediated transformation onto the second chromosome (attP40).

Genomic Sequencing—DNA isolation was performed using Qiagen DNeasy Blood and Tissue kit. 50 adult $shk1^{GM163}/shk1^{GM130}$ flies were used. Isolated DNA at a concentration of > 20ng/μL was sent to BGI Genomics for sequencing. Sequencing was performed using the Hiseq 4000 experimental platform with read lengths of 150PE. Standard bioinformatics procedures were used to generate alignments, assemblies, and SNP calling.

Embryo Processing—For live imaging experiments, after collection, embryos were dechorionated with 50% bleach for 1 minute, rinsed twice with water, placed in halocarbon oil on a gas-permeable membrane, and covered with a glass coverslip.

For fixed embryo experiments, after collection, embryos were dechorionated with 50% bleach for 1 minute, rinsed with water, placed in a fixation solution (8mL nuclease-free water, 1mL 10× PBS, 1mL 37% formaldehyde, and 10mL heptane) in a scintillation vial, and shaken for 20 minutes. The bottom aqueous phase was then removed, 10mL methanol was added, and the vial was shaken forcefully for 30 seconds to remove the vitelline membrane. Embryos were then removed with a pipette from the methanol layer. Embryos were then washed three times with methanol and stored at −20°C in a microcentrifuge tube for < 3 days before staining. Fixed embryos were blocked with 1% BSA/0.1% Tween in PBS three times for 10 minutes each and stained with DAPI at 1μg/mL for 20 minutes. Stained embryos were rinsed twice for 15 minutes in a 1% BSA/0.1% Tween PBS solution followed by a 15-minute rinse in a 0.1% Tween PBS solution. Embryos were mounted on slides with Aquapolymount, covered with glass cover slides, and stored at 4°C.

Microscopy—Images were acquired through confocal microcopy using a Leica SP8 confocal microscope and its software, Leica Application Suite X, using a 20x/0.75 numerical aperture air objective, an argon ion laser and either a 405nm diode laser (for DAPI stained embryos) or a 561nm diode laser (for live imaged embryos).

For imaging cytoplasmic flows, z-stack images (800 × 300 pixels, pixel size 0.73μm) were acquired in ~10μm steps from the cortex to the center of the embryo with a frame rate of 1/7.14s. For imaging the FRET and Rho sensors as well as myosin accumulation, images (800 × 300 pixels, pixel size 0.56μm) were acquired at the cortex of the embryo with a frame rate of ~1/4s. For fixed embryo experiments, single images (800 × 300 pixels, pixel size 0.97) were acquired near the center of the embryo to visualize DAPI stained nuclei. Embryos were screened for current cell cycle at the time of imaging by counting the number of nuclei in the embryo, and only those embryos fixed during cc 6 were imaged.

QUANTIFICATION AND STATISTICAL ANALYSIS

Image Analysis—All image analysis steps were performed using custom-written MATLAB algorithms unless otherwise noted. Confocal images were exported as .tif files from LAS AF software for use in MATLAB algorithms.

Quantification of Nuclear Spreading—Following image acquisition of fixed and DAPI stained embryos, individual nuclei were manually segmented. The convex hull of the set of nuclei was calculated from which the length of the nuclear cloud was obtained. The ratio of this length to the length of the entire embryo became the metric for the degree of nuclear spreading in an embryo. This analysis was performed with all genotypes listed and the nonparametric Kolmogorov–Smirnov statistical test was used to compare the distributions of nuclear spreading.

Quantification of Cytoplasmic Flows and PIV—Following image acquisition of z-stack timeseries, the ~4 z-slices (a vertical distance of ~30μm) towards the center of the embryo were isolated, and a maximum projection of the data was performed. This yielded a timeseries with one image channel with stained yolk (to calculate cytoplasmic flows) and one image channel with PCNA-TagRFP (to calculate nuclear movement). To further smooth the data to be used in particle image velocimetry and to ensure nuclei had moved between each time point, each image in the time series was averaged with its temporal neighbors. One thousand random points were distributed across the embryo which became the initial points for PIV (for PIV using the nuclei, the centroids of the nuclei became the initial points). For each time point, the correlation between the fluorescence in a 35 × 35px square around each point and neighboring regions in the next time point was calculated, and the location of the highest correlation yielded the trajectory of the cytoplasm or nuclei for each time point. To generate heatmaps of the cytoplasmic flows for visualization, the trajectories were discretized across the AP axis in 8-pixel wide bins for each time point. This data set was then smoothed using a Savitzky–Golay filter with a 3rd degree polynomial over 45 time points for visualization.

Quantification of the N/C ratio—To quantify the N/C ratio in neighborhoods of different sizes, we discretized embryos containing His-RFP with grid points every 10px (5.6μm) to give 2400 (80 × 30) grid points in the 800 × 300px image domain. Grid points outside the embryo were discarded. We selected the frame either ~5 minutes before a mitotic division began (when all nuclei were immobile following the previous mitotic division) or ~ 5 minutes after the embryo had halted at the MBT (as defined by no mitotic events for >~20 minutes at cc 14). At that time point, the nuclei were segmented using MATLAB's adaptive thresholding function adaptthresh with a sensitivity of 0.35, and a mask of the entire embryo was generated manually. Regions of the embryo where nuclear segmentation was poor (due to being slightly out of focus for example) were discarded. The N/C ratio was then calculated as the number of nuclei within a value for the community radius divided by the area of embryo within that same distance. We then normalized that value by the embryo-wide average N/C ratio at cc 14 in normally dividing embryos.

N/C Ratio Threshold Models—After calculating the N/C ratio in a region and scoring whether that region had divided, we tested different models to determine their ability to predict division behavior. We used a training data set consisting of 33 embryos, 15 in which the entire embryo divided, 12 of which none of the embryo divided, and 6 of which only part of the embryo divided to fit parameters in these models and a test data set of 6 embryos in which only part of the embryo divided to determine predictive ability.

For a simple threshold model, we fit the N/C ratio and division behavior data to a logistic curve and used the N/C ratio value at which the curve crossed 50% as the single parameter in the model, P_1. This model predicted that if a region had a local N/C ratio below that threshold value, it should undergo a mitotic division. We then considered whether adding some variance in the threshold between embryo would yield a better model. For this model we varied the threshold for each embryo individually and chose the best threshold in the range $P_1/(1+a)$ to $P_1*(1+a)$ where a takes the value of 0, 0.05, 0.1, 0.2, and 1 in Figure S3G.

We next considered a model with a global threshold which decreases with time, starting when the first nucleus divides (Fig S3H). This model might reflect the fact that Cdc25 is degraded at the MBT, in principle reducing the likelihood of nuclei dividing after some time and increasing the likelihood of generating embryos with a portion undergoing an extra division. This model contained two parameters which were fit to the training data consisting of the initial N/C ratio threshold at time = 0 (tested uniformly between 0 and ~1.15) and the rate of threshold decrease with time (tested uniformly between 0 and ~0.4), both parameters relative to the average N/C ratio at cc 14 in normally dividing embryos.

We finally tested a model with a threshold which had some slight gradient across the AP axis. This model contained two parameters, where the threshold T at a certain point x across the AP axis is given as $T = mx + b$. In Figure S3I, the parameters are fit to the training data set. By allowing both parameters to vary slightly between embryos, a much better prediction could be made (Figure 4C). Specifically, m is constrained such that the threshold at the posterior is no more than 10% higher than the threshold at the anterior.

Compound Chromosome Embryo Analysis—To generate embryos with altered DNA content, we first used the C(2)EN^{+} stock which is known to give very few embryos with three copies of chromosome 2 (triplo-2, about 1%).[59] Using this stock, we could be confident of the cell cycle timing of embryos with only one copy of chromosome 2 (haplo-2). We found that these embryos had consistently faster cell cycles 12 and 13 than wild type. Next, we repeated the experiments with C(2)EN$^{b\ pr}$ which is expected to have a significant fraction of triplo-2 embryos (roughly 40%).[59] We observed about 40% of embryos which had longer cell cycles 12 and 13 and never did an extra division.[10] Thus, we have assumed that those embryos are triplo-2. While the same approach could not be performed with the C(3)EN stocks, as they both give haplo-3 and triplo-3, we naturally extended the reasoning for chromosome 2 and found that the duration of cell cycle 12 and 13 could be easily clustered into two separate groups which we interpreted as haplo and triplo-3 (Figure S4). These stocks giving roughly equal numbers of haplo-2/3 and triplo-2/3 were used for experiments.

Quantification of Biosensors and Cdk1 Activation Rates—Fluorescence intensity of Rho and myosin images were averaged across the embryo cortex in each time frame. Cdk1 FRET curves were computed by taking the fluorescence intensity ratio of YFP signal over CFP signal (the emission ratio). To correct for slight out-of-focus shifting and embryo drift, the data were normalized and detrended as in previous work.[3] This signal was averaged over the entire embryo cortex in Figure 4I and in rectangles of width 22.4μm across the AP axis in Figure S1. To determine whether there was a difference in Cdk1 activation rates across the AP axis (Figure 4J, K), the emission ratio was averaged in neighborhoods of 40μm in a grid divided evenly across the embryo. S phase Cdk1 activation rates were computed by fitting a straight line through the first ~5 min of Cdk1 activity increase after the last mitotic division finished at the beginning of cc 14 (Figure 4I) or at mitosis of cc 13 (Figure 4J, K). The F test was used to compare Cdk1 activation rates across the AP axis to test the significance of a non-zero slope term over the naive model with only the intercept parameter.

Mathematical Modeling—We modified a mathematical model of Cdk1 activity[24] to introduce a gradient of N/C ratio across the AP axis. The model reads:

$$\frac{\partial a(x,t)}{\partial t} = D\nabla^2 a(x,t) + G(a,t) + \eta(x,t)$$

where

$$G(a,t) = G_0[\alpha + r_+(a)(c(t) - a) - r_-(a)a]$$

and

$$r_+(a) = \left(c_0 + c_1\frac{a^n}{K_{Cdc25}^n + a^n}\right)\left(1 - h_0(x)\frac{K_{Chk1}^s}{K_{Chk1}^s + a^s}\right)\left(\frac{1}{1 + \left(\frac{t}{t_0}\right)^5}\right)$$

$$r_-(a) = h_0(x)\left(w_0 + w_1\frac{K_{Wee1}^n}{K_{Wee1}^n + a^n}\frac{K_{Chk1}^s}{K_{Chk1}^s + a^s}\right)$$

The quantity $c(t) = \alpha t$ denotes the total amount of Cyclin-Cdk1 complexes, so that the difference $c(t) - a(x, t)$ reflects the amount of inactive Cdk1. The first term in $r_+(a)$ describes the positive feedback between Cdk1 and Cdc25, the second term the negative regulation of Cdc25 by Chk1 and the negative feedback of Cdk1 on Chk1, the third, time-dependent term models the degradation of Cdc25 at cycle 14 which is required for cell cycle lengthening at cycle 14.[51,60] The $r_-(a)$ describes the double negative feedback between Cdk1 and Wee1, the modulation of Wee1 activity by Chk1 and the negative feedback of Cdk1 on Chk1. Note that our model focuses on the activation of Cdk1 and does not explicitly model its inactivation at the exit from mitosis. The rationale is that we have previously shown that the exit from

mitosis is controlled by a phase wave that reflects the delays set by the earlier Cdk1 wave, which times the entry into mitosis.[10] The noise term is a Langevin, Gaussian noise with short spatiotemporal correlations:

$$\langle \eta(x,t)\eta(x',t')\rangle = \sigma^2 G_0[\alpha + r_+(a)(c(t)-a) - r_-(a)a]\delta(x-x')\delta(t-t')$$

A gradient of N/C ratio was introduced by defining $h_0(x)$ as a piecewise linear, noisy gradient:

$$h_0(x) = \begin{cases} h_0 + h_1\left(1 - \frac{x}{0.7}\right) + \xi(x) \; for \; x < 0.7 \\ h_0 + \xi(x) \; for \; x \geq 0.7 \end{cases}$$

where x is the normalized position along the Anterior-Posterior Axis ($x = 0$ at the Anterior pole and $x = 1$ at the Posterior pole) and $\xi(x)$ is a brown noise term ($\frac{1}{f^2}$ spectrum) with $\langle \xi(x) \rangle = 0$ and $\langle \xi^2(x) \rangle = \Gamma^2$, generated using the MATLAB function dsp.ColoredNoise. The stochastic model was simulated using finite differences and Euler method with reflecting boundary conditions. The parameters used are listed in Table S1.

Supplementary Material

Refer to Web version on PubMed Central for supplementary material.

Acknowledgments

We thank the Bloomington *Drosophila* Stock Center, the Kyoto *Drosophila* Stock Center, Ruth Lehmann, Denise Montell and Alana O'Reilly for providing stocks. We thank the *Drosophila* Genomics Resource Center for constructs. We thank members of the Di Talia lab for comments on the manuscript. This work was supported by a Schlumberger Faculty for the Future Fellowship and an HHMI International Student Research Fellowship to V.D., Associazione Italiana Ricerca sul Cancro (AIRC) MFAG-2020 n. 25040 to A.P.; University of Torino Fondo Ricerca Locale 2019 and 2020 PULA_RILO_19_01 and PULA_RILO_2020 to A.P., and NIH (R01-GM122936 and R01-GM136763) to S.D.

References

1. Gerhart JC (1980). Mechanisms Regulating Pattern Formation in the Amphibian Egg and Early Embryo. In Biological Regulation and Development, Goldberger R, ed. (Plenum Press), pp. 133–316.
2. Zalokar M, and Erk I (1976). Division and migration of nuclei during early embryogenesis of Drosophila melanogaster. J.Microsc.Biol.Cell. 25, 97–106.
3. Deneke VE, Puliafito A, Krueger D, Narla AV, De Simone A, Primo L, Vergassola M, De Renzis S, and Di Talia S (2019). Self-Organized Nuclear Positioning Synchronizes the Cell Cycle in *Drosophila* Embryos. Cell 177, 925–941.e917. 10.1016/j.cell.2019.03.007. [PubMed: 30982601]
4. Yohn CB, Pusateri L, Barbosa V, and Lehmann R (2003). l (3) malignant brain tumor and three novel genes are required for Drosophila germ-cell formation. Genetics 165, 1889–1900. [PubMed: 14704174]
5. Hatanaka K, and Okada M (1991). Retarded nuclear migration in Drosophila embryos with aberrant F-actin reorganization caused by maternal mutations and by cytochalasin treatment. Development 111, 909–920. 10.1242/dev.111.4.909. [PubMed: 1879360]

6. Sarikas A, Hartmann T, and Pan Z-Q (2011). The cullin protein family. Genome Biology 12, 220. 10.1186/gb-2011-12-4-220. [PubMed: 21554755]
7. Alphey L, Jimenez J, White-Cooper H, Dawson I, Nurse P, and Glover DM (1992). twine, a cdc25 homolog that functions in the male and female germline of drosophila. Cell 69, 977–988. 10.1016/0092-8674(92)90616-K. [PubMed: 1606618]
8. Royou A, Sullivan W, and Karess R (2002). Cortical recruitment of nonmuscle myosin II in early syncytial Drosophila embryos: its role in nuclear axial expansion and its regulation by Cdc2 activity. The Journal of cell biology 158, 127–137. [PubMed: 12105185]
9. Munjal A, Philippe J-M, Munro E, and Lecuit T (2015). A self-organized biomechanical network drives shape changes during tissue morphogenesis. Nature 524, 351–355. [PubMed: 26214737]
10. Deneke Victoria E., Melbinger A, Vergassola M, and Di Talia S (2016). Waves of Cdk1 Activity in S Phase Synchronize the Cell Cycle in Drosophila Embryos. Developmental Cell 38, 399–412. 10.1016/j.devcel.2016.07.023. [PubMed: 27554859]
11. Gavet O, and Pines J (2010). Progressive Activation of CyclinB1-Cdk1 Coordinates Entry to Mitosis. Developmental Cell 18, 533–543. 10.1016/j.devcel.2010.02.013. [PubMed: 20412769]
12. Okumura F, Joo-Okumura A, Nakatsukasa K, and Kamura T (2016). The role of cullin 5-containing ubiquitin ligases. Cell Division 11, 1. 10.1186/s13008-016-0016-3. [PubMed: 27030794]
13. Laszlo GS, and Cooper JA (2009). Restriction of Src Activity by Cullin-5. Current Biology 19, 157–162. 10.1016/j.cub.2008.12.007. [PubMed: 19147357]
14. Pan Q, Qiao F, Gao C, Norman B, Optican L, and Zelenka PS (2011). Cdk5 targets active Src for ubiquitin-dependent degradation by phosphorylating Src(S75). Cellular and Molecular Life Sciences 68, 3425. 10.1007/s00018-011-0638-1. [PubMed: 21442427]
15. Teckchandani A, Laszlo GS, Simó S, Shah K, Pilling C, Strait AA, and Cooper JA (2014). Cullin 5 destabilizes Cas to inhibit Src-dependent cell transformation. Journal of Cell Science 127, 509–520. 10.1242/jcs.127829. [PubMed: 24284072]
16. Hakak Y, and Martin GS (1999). Ubiquitin-dependent degradation of active Src. Current Biology 9, S1–1042. 10.1016/S0960-9822(99)80453-9.
17. Harris KF, Shoji I, Cooper EM, Kumar S, Oda H, and Howley PM (1999). Ubiquitin-mediated degradation of active Src tyrosine kinase. Proceedings of the National Academy of Sciences 96, 13738–13743.
18. Imamoto A, and Soriano P (1993). Disruption of the csk gene, encoding a negative regulator of Src family tyrosine kinases, leads to neural tube defects and embryonic lethality in mice. Cell 73, 1117–1124. 10.1016/0092-8674(93)90641-3. [PubMed: 7685657]
19. Brown MT, and Cooper JA (1996). Regulation, substrates and functions of src. Biochimica et biophysica acta 1287 2–3, 121–149. [PubMed: 8672527]
20. O'Reilly AM, Ballew AC, Miyazawa B, Stocker H, Hafen E, and Simon MA (2006). Csk differentially regulates Src64 during distinct morphological events in Drosophila germ cells. Development 133, 2627–2638. 10.1242/dev.02423. [PubMed: 16775001]
21. Boschek CB, Jockusch BM, Friis RR, Back R, Grundmann E, and Bauer H (1981). Early changes in the distribution and organization of microfilament proteins during cell transformation. Cell 24, 175–184. 10.1016/0092-8674(81)90513-4. [PubMed: 6263486]
22. Pedraza LG, Stewart RA, Li D-M, and Xu T (2004). Drosophila Src-family kinases function with Csk to regulate cell proliferation and apoptosis. Oncogene 23, 4754–4762. 10.1038/sj.onc.1207635. [PubMed: 15107833]
23. Idema T, Dubuis JO, Kang L, Manning ML, Nelson PC, Lubensky TC, and Liu AJ (2013). The Syncytial Drosophila Embryo as a Mechanically Excitable Medium. PLOS ONE 8, e77216. 10.1371/journal.pone.0077216. [PubMed: 24204774]
24. Vergassola M, Deneke VE, and Di Talia S (2018). Mitotic waves in the early embryogenesis of Drosophila: Bistability traded for speed. Proceedings of the National Academy of Sciences 115, E2165–E2174. 10.1073/pnas.1714873115.
25. Lu X, Li JM, Elemento O, Tavazoie S, and Wieschaus EF (2009). Coupling of zygotic transcription to mitotic control at the Drosophila mid-blastula transition. Development 136, 2101–2110. 10.1242/dev.034421. [PubMed: 19465600]

26. Edgar BA, Kiehle CP, and Schubiger G (1986). Cell cycle control by the nucleo-cytoplasmic ratio in early Drosophila development. Cell 44, 365–372. 10.1016/0092-8674(86)90771-3. [PubMed: 3080248]
27. Yasuda GK, Baker J, and Schubiger G (1991). Temporal regulation of gene expression in the blastoderm Drosophila embryo. Genes & Development 5, 1800–1812. 10.1101/gad.5.10.1800. [PubMed: 1680772]
28. Strong IJT, Lei X, Chen F, Yuan K, and O'Farrell PH (2020). Interphase-arrested Drosophila embryos activate zygotic gene expression and initiate mid-blastula transition events at a low nuclear-cytoplasmic ratio. PLOS Biology 18, e3000891. 10.1371/journal.pbio.3000891. [PubMed: 33090988]
29. Chang JB, and Ferrell JE Jr (2013). Mitotic trigger waves and the spatial coordination of the Xenopus cell cycle. Nature 500, 603–607. [PubMed: 23863935]
30. Novak B, and Tyson JJ (1993). Modeling the cell division cycle: M-phase trigger, oscillations, and size control. Journal of theoretical biology 165, 101–134.
31. Fogarty P, Campbell SD, Abu-Shumays R, Phalle B.d.S., Yu KR, Uy GL, Goldberg ML, and Sullivan W (1997). The Drosophila grapes gene is related to checkpoint gene chk1/rad27 and is required for late syncytial division fidelity. Current Biology 7, 418–426. 10.1016/S0960-9822(06)00189-8. [PubMed: 9197245]
32. Sibon OCM, Stevenson VA, and Theurkauf WE (1997). DNA-replication checkpoint control at the Drosophila midblastula transition. Nature 388, 93–97. 10.1038/40439. [PubMed: 9214509]
33. Shimuta K, Nakajo N, Uto K, Hayano Y, Okazaki K, and Sagata N (2002). Chk1 is activated transiently and targets Cdc25A for degradation at the Xenopus midblastula transition. The EMBO journal 21, 3694–3703. [PubMed: 12110582]
34. Brouns MR, Matheson SF, and Settleman J (2001). p190 RhoGAP is the principal Src substrate in brain and regulates axon outgrowth, guidance and fasciculation. Nature Cell Biology 3, 361–367. 10.1038/35070042. [PubMed: 11283609]
35. DerMardirossian C, Rocklin G, Seo J-Y, and Bokoch GM (2006). Phosphorylation of RhoGDI by Src regulates Rho GTPase binding and cytosol-membrane cycling. Mol Biol Cell 17, 4760–4768. 10.1091/mbc.e06-06-0533. [PubMed: 16943322]
36. Nagao M, Kaziro Y, and Itoh H (1999). The Src family tyrosine kinase is involved in Rho-dependent activation of c-Jun N-terminal kinase by Gα12. Oncogene 18, 4425–4434. 10.1038/sj.onc.1202832. [PubMed: 10442633]
37. Newport J, and Kirschner M (1982). A major developmental transition in early xenopus embryos: I. characterization and timing of cellular changes at the midblastula stage. Cell 30, 675–686. 10.1016/0092-8674(82)90272-0. [PubMed: 6183003]
38. Newport J, and Kirschner M (1982). A major developmental transition in early xenopus embryos: II. control of the onset of transcription. Cell 30, 687–696. 10.1016/0092-8674(82)90273-2. [PubMed: 7139712]
39. Masui Y, and Wang P (1998). Cell cycle transition in early embryonic development of Xenopus laevis. Biology of the Cell 90, 537–548. 10.1111/j.1768-322X.1998.tb01062.x. [PubMed: 10068998]
40. Edgar BA, and Schubiger G (1986). Parameters controlling transcriptional activation during early drosophila development. Cell 44, 871–877. 10.1016/0092-8674(86)90009-7. [PubMed: 2420468]
41. Chan SH, Tang Y, Miao L, Darwich-Codore H, Vejnar CE, Beaudoin J-D, Musaev D, Fernandez JP, Benitez MDJ, Bazzini AA, et al. (2019). Brd4 and P300 Confer Transcriptional Competency during Zygotic Genome Activation. Developmental Cell 49, 867–881.e868. 10.1016/j.devcel.2019.05.037. [PubMed: 31211993]
42. Lee MT, Bonneau AR, Takacs CM, Bazzini AA, DiVito KR, Fleming ES, and Giraldez AJ (2013). Nanog, Pou5f1 and SoxB1 activate zygotic gene expression during the maternal-to-zygotic transition. Nature 503, 360–364. 10.1038/nature12632. [PubMed: 24056933]
43. Pálfy M, Joseph SR, and Vastenhouw NL (2017). The timing of zygotic genome activation. Current Opinion in Genetics & Development 43, 53–60. 10.1016/j.gde.2016.12.001. [PubMed: 28088031]

44. Gert KR, Quio LEC, Novatchkova M, Guo Y, Cairns BR, and Pauli A (2021). Reciprocal zebrafish-medaka hybrids reveal maternal control of zygotic genome activation timing. bioRxiv, 2021.2011.2003.467109. 10.1101/2021.11.03.467109.
45. Jevtić P, and Levy DL (2017). Both Nuclear Size and DNA Amount Contribute to Midblastula Transition Timing in Xenopus laevis. Scientific Reports 7, 7908. 10.1038/s41598-017-08243-z. [PubMed: 28801588]
46. Jevtić P, and Levy DL (2015). Nuclear size scaling during Xenopus early development contributes to midblastula transition timing. Curr Biol 25, 45–52. 10.1016/j.cub.2014.10.051. [PubMed: 25484296]
47. Syed S, Wilky H, Raimundo J, Lim B, and Amodeo AA (2021). The nuclear to cytoplasmic ratio directly regulates zygotic transcription in Drosophila through multiple modalities. Proc Natl Acad Sci U S A 118, e2010210118. 10.1073/pnas.2010210118. [PubMed: 33790005]
48. Lee MT, Bonneau AR, and Giraldez AJ (2014). Zygotic Genome Activation During the Maternal-to-Zygotic Transition. Annual Review of Cell and Developmental Biology 30, 581–613. 10.1146/annurev-cellbio-100913-013027.
49. Pritchard DK, and Schubiger G (1996). Activation of transcription in Drosophila embryos is a gradual process mediated by the nucleocytoplasmic ratio. Genes & Development 10, 1131–1142. 10.1101/gad.10.9.1131. [PubMed: 8654928]
50. Jukam D, Kapoor RR, Straight AF, and Skotheim JM (2021). The DNA-to-cytoplasm ratio broadly activates zygotic gene expression in Xenopus. Current Biology 31, 4269–4281.e4268. 10.1016/j.cub.2021.07.035. [PubMed: 34388374]
51. Farrell JA, and O'Farrell PH (2014). From Egg to Gastrula: How the Cell Cycle Is Remodeled During the Drosophila Mid-Blastula Transition. Annual Review of Genetics 48, 269–294. 10.1146/annurev-genet-111212-133531.
52. Blythe Shelby A., and Wieschaus Eric F. (2015). Zygotic Genome Activation Triggers the DNA Replication Checkpoint at the Midblastula Transition. Cell 160, 1169–1181. 10.1016/j.cell.2015.01.050. [PubMed: 25748651]
53. Lu X, Drocco J, and Wieschaus EF (2010). Cell cycle regulation via inter-nuclear communication during the early embryonic development of Drosophila melanogaster. Cell Cycle 9, 2908–2910. 10.4161/cc.9.14.12346. [PubMed: 20647771]
54. Liu B, Winkler F, Herde M, Witte C-P, and Großhans J (2019). A link between deoxyribonucleotide metabolites and embryonic cell-cycle control. Current Biology 29, 1187–1192. e1183. [PubMed: 30880011]
55. Djabrayan NJV, Smits CM, Krajnc M, Stern T, Yamada S, Lemon WC, Keller PJ, Rushlow CA, and Shvartsman SY (2019). Metabolic Regulation of Developmental Cell Cycles and Zygotic Transcription. Current Biology 29, 1193–1198.e1195. 10.1016/j.cub.2019.02.028. [PubMed: 30880009]
56. Shindo Y, and Amodeo AA (2021). Excess histone H3 is a competitive Chk1 inhibitor that controls cell-cycle remodeling in the early Drosophila embryo. Current Biology 31, 2633–2642.e2636. 10.1016/j.cub.2021.03.035. [PubMed: 33848457]
57. Gilbert SF (2000). Developmental biology (Sinauer Associates).
58. Blankenship JT, and Wieschaus E (2001). Two new roles for the Drosophila AP patterning system in early morphogenesis. Development 128, 5129–5138. 10.1242/dev.128.24.5129. [PubMed: 11748148]
59. Dernburg AF, Daily DR, Yook KJ, Corbin JA, Sedat JW, and Sullivan W (1996). Selective loss of sperm bearing a compound chromosome in the Drosophila female. Genetics 143, 1629–1642. 10.1093/genetics/143.4.1629. [PubMed: 8844151]
60. Di Talia S, She R, Blythe Shelby A., Lu X, Zhang Qi F., and Wieschaus Eric F. (2013). Posttranslational Control of Cdc25 Degradation Terminates Drosophila's Early Cell-Cycle Program. Current Biology 23, 127–132. 10.1016/j.cub.2012.11.029.738 [PubMed: 23290553]

Highlights

- Cullin-5 controls nuclear positioning in *Drosophila* embryos
- Cullin-5 regulates cortical actomyosin contractility
- Nuclei sense the N/C ratio in large collectives and in a spatially graded manner
- Collective sensing of the N/C ratio is required for the robustness of the MBT

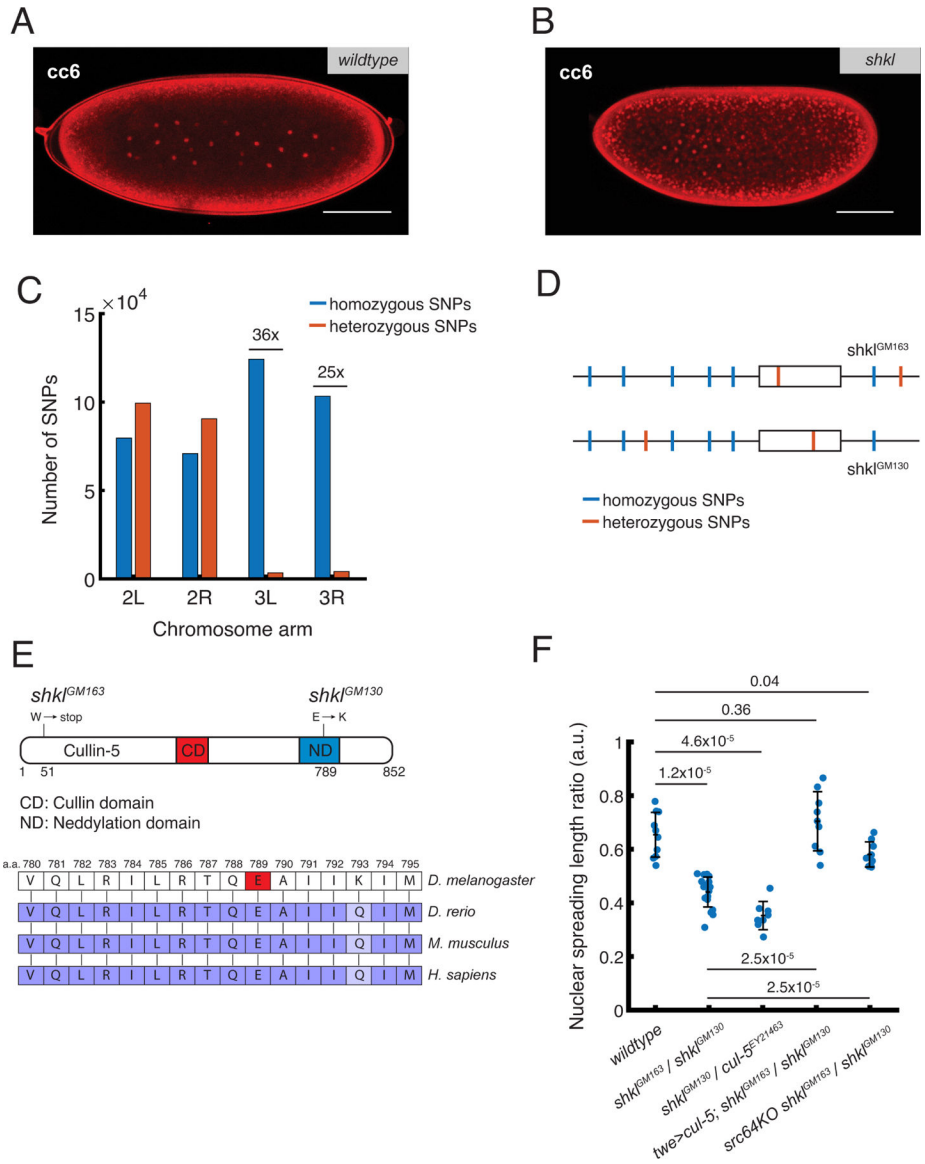

Figure 1. Genetic identification of *shkl* mutants.

(A, B) Nuclear positioning in interphase of cc 6 in wildtype (A) and *shkl* (B) embryos, visualized with PCNA-TagRFP. (C) Number of homozygous and heterozygous SNPs (relative to the reference genome) in *shkl* embryos in each arm of chromosome 2 and 3. The mutant screen[4] was performed on an isogenic third chromosome and thus only the third chromosome has reduced heterozygous SNPs. (D) A theoretical example gene with heterozygous SNPs between the two *shkl* alleles. (E) Top: Schematic for the Cul-5 protein with domains and *shkl* mutations shown. The *GM130* allele of *shkl* contains a point mutation in the neddylation domain where it is evolutionarily conserved. The *GM163* allele contains a point mutation leading to an early stop codon. Bottom: Part of the neddylation domain of the Cul-5 protein in different model organisms. Highlighted residue indicates *GM130* mutation site. (F) Genetic complementation and rescue tests. Fixed embryos were stained with DAPI to show nuclear positioning at cc 6. The ratio between the length of

the nuclear cloud and the length of the embryo was measured. Data are represented as mean ± SEM. P-values (Kolmogorov–Smirnov test) are shown. Each dot represents one embryo. *cul-5*^{EY21463} is a hypomorphic mutant allele. *twe>cul-5* is a transgenic line carrying a plasmid with *cul-5* cDNA under the regulation of the *twine* promotor. Scale bar: 100μm. See also Figure S1 and Video S1.

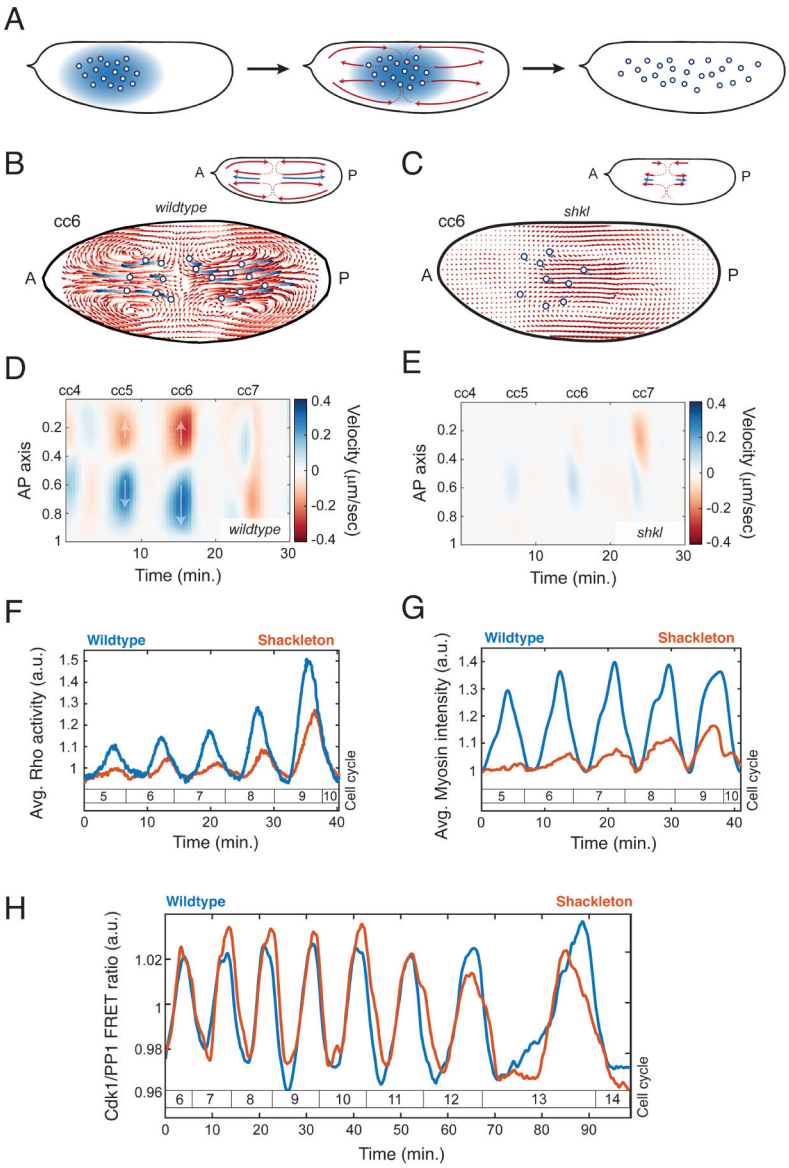

Figure 2. Characterization of the Cul-5 pathway.

(A) Pathway for self-organized nuclear positioning in wildtype embryos; PP1 activity spreads from nuclei to the embryo cortex where it leads to gradients of myosin accumulation, thus generating cytoplasmic flows. These flows position nuclei uniformly across the AP axis. (B, C) PIV in wildtype (B) and *shkl* (C) embryos showing reduced cytoplasmic flows and nuclear movement in *shkl* embryos. Top insets depict magnitude and directionality of flows. (D, E) Heatmap quantification of the cytoplasmic flows in wildtype (D) and *shkl* (E) embryos. Arrows depict directionality of flows. (F, G) Both cortical Rho activity (F) and cortical myosin accumulation (G) are reduced in *shkl* embryos. (H) Cortical oscillations of the Cdk1/PP1 ratio from the FRET biosensor are similar in wildtype and *shkl* embryos. See also Figure S2.

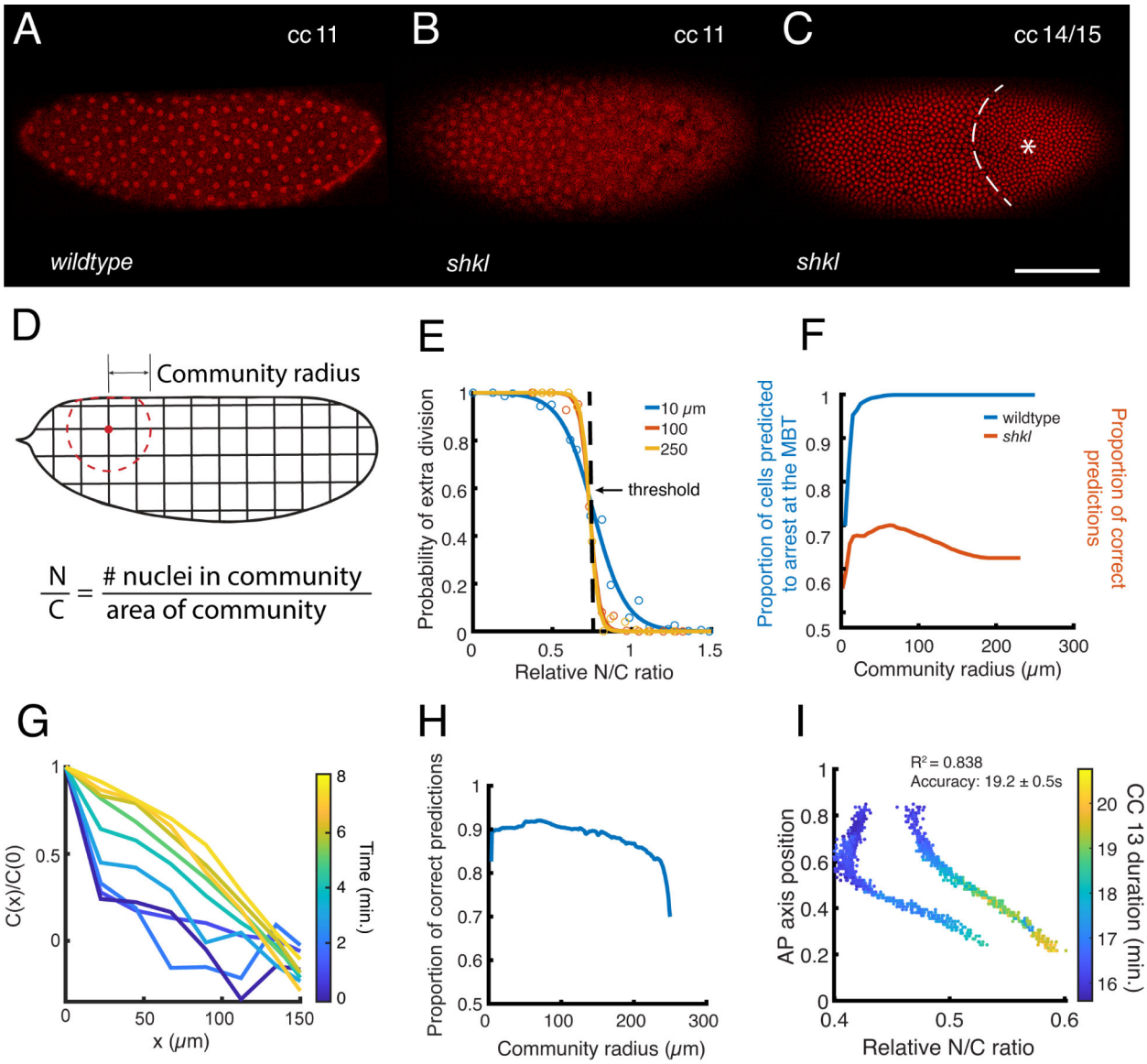

Figure 3. Sensing of the N/C ratio in *shkl* embryos.

(A, B) Positioning of nuclei at cc 11 in wildtype (A) and *shkl* (B) embryos, visualized with His-RFP. (C) A *shkl* embryo at the MBT. The gradient of N/C ratio in *shkl* embryos frequently leads to the posterior undergoing an extra division. Dashed line: boundary between the normal and extra division regions. Asterisk: The region of the embryo which underwent an additional division. (D) Schematic of experimental design. Each embryo was discretized in a grid and a region with a certain community radius was specified. The N/C ratio was calculated as the number of nuclei in the community divided by the area. (E) The probability of a region dividing as a function of the local N/C ratio, relative to the average N/C ratio in wildtype embryos at cc 14. Curves for local neighborhoods of 10, 100, and 250μm are shown. A simple predictive model is a constant N/C ratio threshold, shown as a dashed line. (F) The proportion of nuclei in wildtype embryos which should arrest at the MBT and the proportion of correct predictions in a test data set of *shkl* embryos using

a simple threshold model as a function of community radius. (G) Two-point correlation function of the Cdk1/PP1 field as a function of distance for embryos in interphase of cell cycle 13. The correlation length was estimated as the point at which the correlation reaches 0.5 at the last time point and occurs at ~100μm. (H) The proportion of correct predictions in the *in silico* data set of 22 embryos with a N/C ratio gradient across the AP axis. (I) Duration of cc 13 in 30μm neighborhoods as a function of N/C ratio and position across the AP axis. Accuracy is the average ± SEM of the error in prediction. Scale bar: 100μm. See also Figure S3.

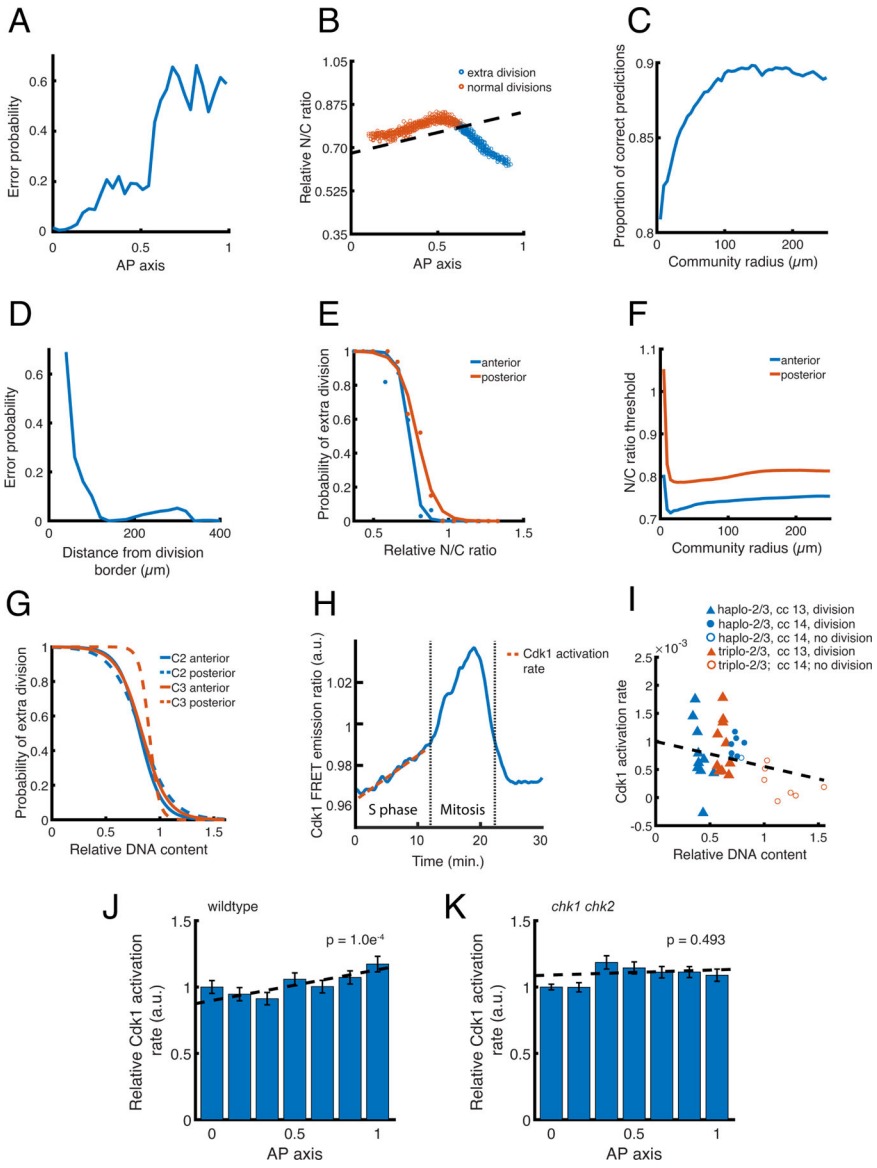

Figure 4. A gradient in N/C ratio sensing across the AP axis.

(A) Errors made by the simple threshold model as a function of position across the AP axis. (B) The N/C ratio in local neighborhoods of 70μm (the maximum of the correct predictions of the simple threshold model) across the AP axis during cc 14. Dashed line shows that an N/C ratio threshold with a slight gradient across the AP axis does a much better job at dividing the normal and extra division regions. (C) This gradient threshold model predicts the division behavior correctly upwards of 90% of the time at a community radius of ~100μm. (D) Errors in prediction from the gradient threshold model are largely near the border between normal and extra division regions. (E) Probability of a region undergoing an extra division as a function of N/C ratio in the anterior third versus posterior third of the embryo at a community radius of 100μm. The posterior curve is shifted towards a higher N/C ratio. (F) The N/C ratio threshold in the anterior and posterior of the embryo at different community radii. (G) Probability of a region undergoing an extra division as a function of

N/C ratio at a community radius of 100μm, performed in embryos with either one additional or one fewer copy of either chromosome 2 or 3. These embryos have altered DNA content but normal nuclear spreading. (H) Diagram showing an oscillation of Cdk1/PP1 FRET ratio during cc 13. The dashed red line indicates a linear fit of the slope of the ratio during S phase which we use as the Cdk1 activation rate. (I) Correlation between Cdk1 activation rate and division behavior in normal and extra division regions in compound chromosome embryos. At low DNA content and high Cdk1 activation rate, nuclei tend to divide. Dashed line: linear fit. (J, K) Cdk1 activation rate across the AP axis (relative to the anterior of the embryo) in wildtype (J) and *chk1 chk2* (K) mutants. Dashed lines indicate linear fit and p values (F-test) for the significance of the slope are shown. Data are represented as mean ± SEM. See also Figure S4.

KEY RESOURCE TABLE

REAGENT or RESOURCE	SOURCE	IDENTIFIER
Chemicals, peptides, and recombinant proteins		
Halocarbon Oil 27	Sigma	Cat # 9002–83–9
Aqua-Poly/Mount	Polysciences, Inc.	Cat # 18606
Deposited data		
Shkl genomic sequencing data	This paper	ID: PRJNA799361
Experimental models: Organisms/strains		
D. melanogaster: w; Cdk1-FRET; His2Av-mRFP	S. Di Talia[10]	N/A
D. melanogaster: w; AniRBD-GFP	T. Lecuit[9]	N/A
D. melanogaster: w[*];; P{w[+mC]=sqh-mCherry.M}3	Bloomington Drosophila Stock Center	BDSC: 59024; FlyBase: FBst0059024
D. melanogaster: w;; PCNA-TagRFP-T	S. Di Talia[10]	N/A
D. melanogaster: w;; shkl ^{GM130} /TM3	R. Lehmann[4]	N/A
D. melanogaster: w;; shkl ^{GM163} /TM3	R. Lehmann[4]	N/A
D. melanogaster: w[1118]	S. Di Talia	Duke University
D. melanogaster: w[1118];; P{w[+mC]=GAL4::VP16-nos.UTR}CG6325[MVD1]	Bloomington Drosophila Stock Center	BDSC: 4937; FlyBasee: FBst0004937
D. melanogaster: w; grp^{209} lok^{30}/grp^{z5170} lok^{30}	J. Sekelsky	N/A
D. melanogaster: w[1118]; P{w[+mC]=UAS-Src42A.CA}5	Bloomington Drosophila Stock Center	BDSC: 6410; FlyBase: FBst0006410
D. melanogaster: w[*]; P{w[+mC]=UAS-Src64B.C}2	Bloomington Drosophila Stock Center	BDSC: 8477; FlyBase: FBst0008477
D. melanogaster: w[*]; TI{w[+mW.hs]=TI}Src64B[ko] P{w[+mW.hs]=FRT(w[hs])}2A/TM6B, Tb[1]	Bloomington Drosophila Stock Center	BDSC: 81022; FlyBase: FBst0081022
D. melanogaster:w; twe > Cul5	This study	N/A
D. melanogaster: y[1] w[67c23]; P{y[+mDint2] w[+mC]=EPgy2}Cul5[EY21463]	Bloomington Drosophila Stock Center	BDSC: 22482; FlyBase: FBst0022482
D. melanogaster: C(2)EN	Bloomington Drosophila Stock Center	BDSC: 2974; FlyBase: FBab0000106
D. melanogaster: C(2)EN, b[1] pr[1]	Bloomington Drosophila Stock Center	BDSC: 1112; FlyBase: FBab0000106
D. melanogaster: C(3)EN, st[1] cu[1] e[s]	Bloomington Drosophila Stock Center	BDSC: 1117; FlyBase: FBab0000131
Software and algorithms		
MATLAB R2020a	Mathworks	N/A